# **LiDAR SLAM Global Positioning Uncertainty Estimation Based on Lie Group and MHSS** theory

Minzhe Liu, Hongjuan Zhang, Bijun Li, Zhibo Zhao
State Key Laboratory of Information Engineering in Surveying, Mapping and Remote Sensing, Wuhan University, Wuhan 430079.
China

Keywords: LiDAR SLAM, Positioning uncertainty, Lie Group theory, MHSS

#### **Abstract**

LiDAR based simultaneous localization and mapping (SLAM) plays an important role for real-time localization and 3D mobile mapping of autonomous systems. However, the long-term scan-to-scan matching in the SLAM can introduce uncertainty into the position estimation, which results in a large drift. In this paper, we specifically focus on real-time estimation of the global positioning uncertainty of LiDAR SLAM so that it can enable the graceful weighting of LiDAR SLAM with other positioning systems in multisensor fusion localization. We introduce Lie group theory and multiple fault hypothesis solution separation (MHSS) method into a Kalman-filter based LiDAR SLAM framework. First, the scan-to-scan matching uncertainty is obtained by establishing fault hypothesis utilizing MHSS method. Then the global positioning uncertainty is propagated on Lie group based on the scan-to-scan matching uncertainty in terms of the relative position and rotation. The NCLT dataset is used to validate the proposed method. Experimental results show that: comparing with previous solutions that treat scan-to-scan matching uncertainty as a constant, the proposed method is more adaptive and robust. And the real-time global positioning uncertainty estimation can envelop the real SLAM absolute trajectory error (ATE) for the most of the time and can reflect the real changing tendency of ATE.

#### 1. Introduction

SLAM technology, since introduced by (Smith et al. 1986), has made great progress and is applied in many fields including autonomous driving, drone guidance, robot positioning and mobile mapping. Depending on the sensors, SLAM methods can be divided into visual SLAM (Macario et al. 2022), LiDAR SLAM (Zou et al. 2022) and multi-sensor fusion SLAM (Tian et al. 2023). LiDAR can obtain high-precision scanning point clouds with depth information and is unaffected by the changes in light conditions so that it has shown broad application prospects in SLAM tasks.

A typical LiDAR SLAM system can be divided into two parts: the front end and the back end. The front end is designed to extract point, edge or planar features (Guo et al. 2022, Tsai et al. 2024). The back end usually performs scan-to-scan matching (e.g. ICP) and optimization process based on the extracted features to calculate the pose transform between scans (Cho et al. 2018). Since the optimization step performed in the back-end is actually the process of calculating the maximum likelihood estimate of the residual error and Jacobian matrix of feature matching, it will inevitably introduce uncertainty in the position estimation. The accumulated uncertainties from continuous matching of multiple scans will make the pose estimation drift away from the true value. The current common solution is to fuse LiDAR SLAM with additional positioning systems (e.g. Global Navigation Satellite System (GNSS), IMU, camera) to provide an integrated solution to improve the positioning accuracy and robustness. For example, the popular LIO-SAM framework (Shan et al. 2020) utilizes the GNSS positioning result as a graph optimization factor to help optimize the LiDAR SLAM to obtain a more accurate pose estimation result. The FAST-LIVO framework and its derivatives (Zheng et al. 2022, Zheng et al. 2024) integrate the camera, LiDAR, and IMU sensors, obtaining robust positioning and mapping results. Therefore, one of the most important aspects of the integrated system is how it models the uncertainty of different positioning modalities (Talbot et al. 2023). This paper focuses on the positioning uncertainty estimation of a Kalman-filter based

LiDAR SLAM framework, and provide a real-time maximum positioning error estimation (upper-limit) during the positioning process.

As two basic LiDAR SLAM frameworks, LOAM (Zhang et al. 2014) and LeGO-LOAM (Shan et al. 2018) both extract edge and planar features and perform scan matching and factor graph optimization to obtain the optimal global pose estimation. The improvement of LeGO-LOAM over LOAM lies in the more refined extraction of edge features and the elimination of outliers. However, they are feature-based methods and may fail in weakly structured scenes. FAST-LIO becomes popular in recent years (Xu et al, 2021. Xu et al, 2022). It directly matches the points in the two scan point clouds and use the Kalman filter framework to iteratively optimize the distance from the point to the nearby plane to obtain the pose result, which makes it more robust in weakly structured scenes. Moreover, they propose a novel filtering method and ikd-tree data structure, which greatly improves the real-time performance. Therefore, we introduce our real-time positioning uncertainty module into FAST-LIO so that it not only estimates global position but also the uncertainty of the global position.

For uncertainty estimation, there have been a series of studies. (Smith et al. 1990) models the motion of the autonomous system as a function of translation and Euler angles, and use the first-order linearization method to calculate the Jacobian matrix. continuous multiplication of Jacobian matrix, it characterizes the error of translation. In more recent study, propagating errors on Lie groups is considered to be a more effective solution (Chirikjian et al. 2009, Chirikjian et al. 2011). (Barfoot et al. 2014) studies the propagation of uncertainty on the SE(3) group by compounding the poses. (Brossard et al. 2022) considers the velocity state and study the propagation of uncertainty on the SE2(3) group. (Mangelson et al. 2020) abandons the assumption that poses are independent to each other and study the error propagation in non-Gaussian distribution and pose-dependent cases through pose inversion. Even though these methods consider non-Gaussian distribution and correlation between poses, they often treat uncertainty of

"Mobile Mapping for Autonomous Systems and Spatial Intelligence", 20-22 June 2025, Xiamen, China

scan-to-scan matching as a constant, which usually undermine the real matching errors.

The main contributions of this paper are as follows:

(1) a self-adapting scan-to-scan matching uncertainty estimation method using MHSS method is proposed, without artificially setting the uncertainty as constant. It constructs fault hypotheses for each LiDAR measurement, calculating the state covariance under each subset, and finally obtains the pose uncertainty of the scan matching. It is then integrated into a Kalman filter based system.

(2) when estimating the global positioning uncertainty, we use the inversion form of the relative pose between two consecutive scans from the scan-to-scan matching, which provides a relative pose transformation for propagating global positioning uncertainty over the SE(3) group, based on above acquired scan-to-scan matching uncertainty estimation.

The effectiveness of our method is verified by the NCLT dataset. Experimental results show that the estimated global positioning uncertainty can envelop the SLAM ATE for the most of the time and can reflect its real changing tendency.

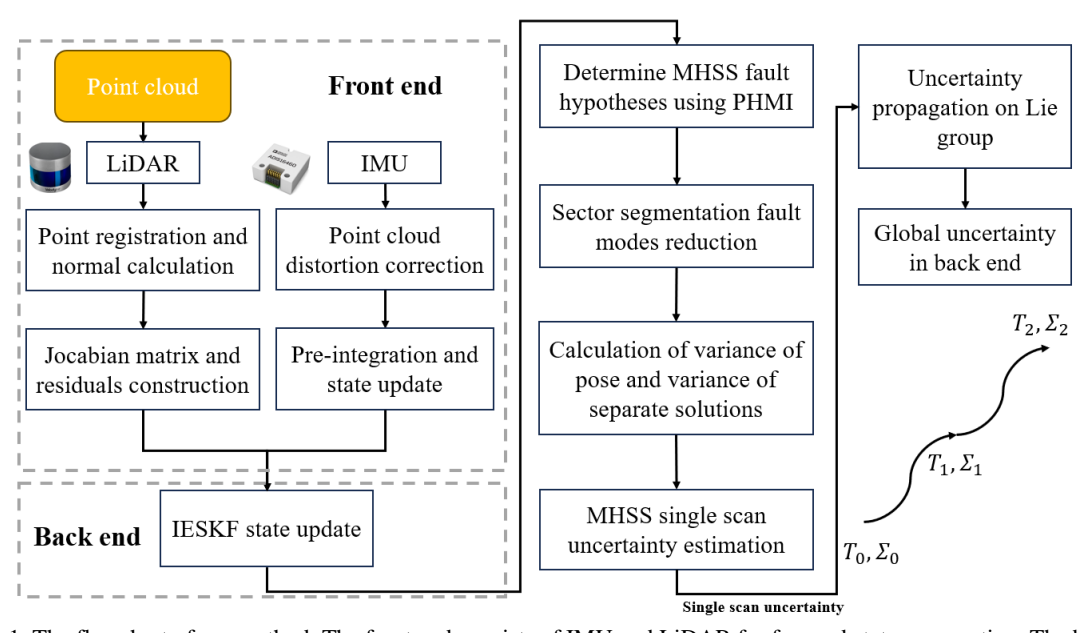


Figure 1. The flowchart of our method. The front end consists of IMU and LiDAR for forward state propagation. The back end updates state with IESKF and we calculate scan matching uncertainty with parameters in optimization procedure.

# 2. Methodology

### 2.1 Overview

Our method is inherited from the LiDAR-Inertial FAST-LIO framework. The role of IMU in the whole filter-based framework is to correct the distorted point cloud and provide the initial pose of the framework. It does not participate in the process of MHSS uncertainty calculation.

Shown as Figure 1, in the front end, the residual and normal vectors of LiDAR points are calculated by point cloud registration. In the back end, we update the state and apply the MHSS module to calculate the uncertainty generated by scanto-scan matching based on Kalman filter. The calculated scanto-scan uncertainty is then used to obtain the global uncertainty through the Lie group propagation.

#### 2.2 State Definition and Filtering Process

Since IMU measurements have a higher frequency than LiDAR, we use the pre-integration to estimate the relative pose between two LiDAR scans:

$$p_{b,i+1}^{W} = p_{b,i}^{W} + v_{b,i}^{W} \Delta t + \frac{1}{2} \overline{a}_{i} \Delta t^{2}$$
 (1)

$$v_{b,i+1}^W = v_{b,i}^W + \overline{a}_i \Delta t \tag{2}$$

$$q_{b,i+1}^{W} = q_{b,i}^{W} \otimes \begin{bmatrix} 1\\ \frac{1}{2} \overline{\omega}_{i} \Delta t \end{bmatrix}$$
 (3)

where W is the world frame. b is the body frame. p is the IMU position, v is the velocity and q is the quaternion representing the rotation. i is the i-th IMU timestamp.

$$\overline{a}_{i} = \frac{1}{2} \left[ q_{i} \left( \hat{a}_{i} - b_{a_{i}} \right) - g^{W} + q_{i+1} \left( \hat{a}_{i+1} - b_{a_{i}} \right) - g^{W} \right]$$
(4)

$$\overline{\omega}_{i} = \frac{1}{2} \left( \hat{\omega}_{i} + \hat{\omega}_{i+1} \right) - b_{\omega_{i}} \tag{5}$$

Where  $\hat{a}$  and  $\hat{\omega}$  are measurement values of the accelerometer and gyroscope.  $b_a$  and  $b_\omega$  are the bias.  $g^W$  is the gravity vector in world frame

The IMU pre-integration is implemented until the new LiDAR scan needs to perform ICP matching, we use iterated error state Kalman filter (IESKF) to optimize state estimation. The state vector is defined as:

$$x = \begin{bmatrix} R_I^W & p_I^W & v_I^W & b_a & b_\omega & g^W \end{bmatrix}$$
 (6)

I represents the IMU body coordinate. The  $R_I^W$ ,  $p_I^W$  and  $v_I^W$  are the transformation vector of the rotation, position, and velocity from the IMU coordinate system to the world coordinate system.

The measurement model can be summarized as:

$$0 = n_j^T \left( R_L^W s_j + q_j \right) \tag{7}$$

where  $n_j^T$  is the corresponding normal vector of point j,  $R_L^W$  is the rotation matrix that projects the point from the LiDAR coordinate to the world coordinate. q is point matching with s.

"Mobile Mapping for Autonomous Systems and Spatial Intelligence", 20–22 June 2025, Xiamen, China

The residual vector is calculated as:

$$r = z - Hx \tag{8}$$

z is the LiDAR measurement while H is the Jacobian matrix acquired by Eq.(7).

The Kalman gain matrix K is:

$$K = PH^{T} \left( HPH^{T} + N \right)^{-1} \tag{9}$$

P is the state variance matrix. N is the measurement noise matrix. The updated state and state variance is:

$$x(+) = x(-) + Kr \tag{10}$$

$$P(+) = (I - KH)P(-) \tag{11}$$

The iteration process stops when the norm of the state update is less than a certain threshold. After the state update, we can get the optimal estimate of the global rotation and position of the LiDAR in the current scan, which enables us to establish the Lie group pose elements in later process.

# 2.3 Scan-to-scan Matching Uncertainty Estimation based on MHSS

In ICP process, the LIDAR measurements inevitably have ranging and angle errors, which will cause the optimal estimation results to be a theoretical maximum likelihood solution, and there is a certain uncertainty between the state estimation and the true value. Regarding this issue, we introduce the MHSS method to estimate the uncertainty introduced by scan-to-scan matching in Eq. (7).

According to MHSS method's step, we establish the following fault hypothesis:

$$FH_0 \quad FH_1 \quad FH_2 \quad FH_3 \quad \cdots \quad FH_j$$

$$\Omega_0 \quad \Omega_1 \quad \Omega_2 \quad \Omega_3 \quad \cdots \quad \Omega_j$$

$$P_{FH_0} \quad P_{FH_1} \quad P_{FH_2} \quad P_{FH_3} \quad \cdots \quad P_{FH_j}$$
(12)

where  $FH_0$  is the fault free hypothesis. This hypothesis means that we will use all LiDAR measurements for state updates.  $\Omega_0$  is state variance of rotation and position and can be extracted from state covariance matrix P(+) in Eq. (11).

$$\Omega_0 = \begin{bmatrix} I_{6\times6} & \\ & 0_{0\times9} \end{bmatrix} P(+) \begin{bmatrix} I_{6\times6} & \\ & 0_{0\times9} \end{bmatrix}^T$$
 (13)

 $P_{FH_0}$  is the probability of fault-free hypothesis occurring.  $FH_j$  is the j-th fault hypothesis which means the j-th measurement exists gross error. When calculating the corresponding state and state covariance under j-th hypothesis, we eliminate the j-th measurement from the whole Jacobian matrix and residual vector from Eq. (7).

After acquiring the variance of the state of the six degrees of freedom  $\Omega$  and the probability  $P_{FH}$ , we can calculate the uncertainty of each state by (Blanch et al. 2012, Blanch et al. 2015):

$$2Q\left(\frac{U_{d}}{\Omega_{0}}\right) + \sum_{j=1}^{N_{\text{fashinedess}}} P_{FH_{j}} Q\left(\frac{U_{d} - Thres_{j,d}}{\Omega_{i}}\right)$$

$$= PHMI\left(1 - \frac{P_{unmonitored}}{PHMI}\right)$$
(14)

where  $U_d$  represents the uncertainty of the corresponding state. PHMI is the integrity risk which represents the upper limit of the probability of all fault hypotheses occurring.  $P_{unmonitored}$  is the unmonitored integrity risk, usually part of the overall integrity risk.  $d=1,\cdots,6$  corresponds to every dimension of the rotation and position states. Q represents the normal distribution. *Thres* is the threshold calculated based on the continuous risk  $P_{fa}$  and is in the form:

$$Thres_{i.d} = K_{fa} \Omega^{j}_{ss.d} \tag{15}$$

$$K_{fa} = Q^{-1} \left( \frac{P_{fa}}{2N_{\text{faultmodes}}} \right) \tag{16}$$

$$\Omega_{ss}^{j} = \Omega_{i}^{2} - \Omega_{0}^{2} \tag{17}$$

After calculating the uncertainty of each rotation and translation, we form a diagonal matrix as the uncertainty introduced by the current scan matching:

$$\sum = diag\left( \begin{bmatrix} U_{tx}^2 & U_{ty}^2 & U_{tz}^2 & U_{rx}^2 & U_{ry}^2 & U_{rz}^2 \end{bmatrix} \right) \quad (18)$$

Where tx, ty, tz represents the translation in corresponding axis while rx, ry, rz is the rotation. Note that the order of the states defined here is different from that in Eq. (6). This is to ensure consistency in propagating uncertainty on Lie group in the following chapter.

#### 2.4 Covariance Propagation on SE(3) Group

In our SLAM framework, the defined states include rotation R and position p. They can be represented by homogeneous matrices of the special Euclidean group:

$$SE(3) = \begin{cases} T = \begin{bmatrix} R & p \\ & I \end{bmatrix} \in \mathbb{R}^{4\times4} \mid \\ R \in SO(3), p \in \mathbb{R}^3 \end{cases}$$
 (19)

SO(3) is the special orthogonal group representing rotation.

In Section 2.2, we obtain the rotation and position estimation results of the previous scan and obtain the rotation and position estimation of the current scan through Kalman filtering in Eq. (10). These two sets of states can be expressed as special Euclidean groups  $T_0$  and  $\hat{T}_1$  through Eq.(19). The propagation of uncertainty requires the change between two pose, so we use the inverse method to obtain it:

$$T_1 = \hat{T}_1 \bullet T_0^{-1} \tag{20}$$

According to the analysis in Section 2.3,  $T_0$  has global uncertainty after propagation, and  $T_1$  has uncertainty introduced by scan matching. Their true value and uncertainty expectation is:

$$\left\{\overline{T}_{0}, \Sigma_{0}\right\}, \left\{\overline{T}_{1}, \Sigma_{1}\right\} \tag{21}$$

Consider the common case where the LiDAR starts moving from rest,  $\Sigma_0$  is the uncertainty of the initial pose, which can be set to a matrix of all zeros.  $\Sigma_1$  is obtained by Eq.(18). The uncertainty of the pose can be expressed as the true transform left multiplied by a small perturbation:

$$T_{0} = \exp\left(\xi_{0}^{\wedge}\right) \overline{T}_{0}$$

$$T_{1} = \exp\left(\xi_{1}^{\wedge}\right) \overline{T}_{1}$$
(22)

For  $\hat{T}_{\!_1}$  which compounds the two poses  $T_{\!_0}$  and  $T_{\!_1}$  , its uncertainty can be written as:

$$\hat{T}_{1} = \exp\left(\xi^{\wedge}\right) \hat{T}_{1} = \exp\left(\xi_{1}^{\wedge}\right) \exp\left(\left(\Gamma_{T_{1}}^{left} \xi_{0}\right)^{\wedge}\right) \overline{T}_{1} \overline{T}_{0} \quad (23)$$

 $\Gamma_T^{left}$  is in the form:

 $\Gamma_{T_1,SE(3)}^{left} = \begin{bmatrix} R & \rho_{\times} R \\ & R \end{bmatrix}$  (24)

 $\left(\right)_{\times}$  is the skew-symmetric matrix of the vector. The state uncertainty covariance matrix  $\sum_{0}$  of pose  $T_{0}$  can be written as:

$$\Sigma_{0,SE(3)} = \begin{bmatrix} \Sigma_{0,\rho\rho} & \Sigma_{0,\rho\phi} \\ \Sigma_{0,\phi\rho} & \Sigma_{0,\phi\phi} \end{bmatrix}$$
 (25)

By propagating the  $\Sigma_0$  with pose  $T_1$ , the covariance matrix will be:

$$\begin{split} & \Sigma_{0}^{\cdot} = \Gamma_{T_{1}}^{left} \Sigma_{0} \Gamma_{T_{1}}^{left, runnspose} = \\ & \left[ \rho_{x} R \Sigma_{\phi\phi} \rho_{x} R + R \Sigma_{\rho\phi} \rho_{x} R + \rho_{x} R \Sigma_{\phi\rho} R + R \Sigma_{\rho\rho} R - R \Sigma_{\rho\phi} R + \rho_{x} R \Sigma_{\phi\phi} R \right] \\ & R \Sigma_{\phi\rho} R + R \Sigma_{\phi\phi} \rho_{x} R - R \Sigma_{\phi\phi} \rho_{x} R \end{split}$$

In chapter 2.3, we introduce how to calculate the scan matching uncertainty  $\xi_1$  of the pose  $T_1$ . By compounding the propagated uncertainty with  $\xi_1$ , we can get the global uncertainty of the current scan, which is in the same form as the Eq.(18). The multiplication of the exponential mapping of  $\exp\left(\xi_1^\wedge\right)\exp\left(\left(\Gamma_{T_i}^{left}\xi_0\right)^\wedge\right)$  is a series of polynomials with specific coefficients which implies that the global uncertainty

specific coefficients which implies that the global uncertainty after propagation in the current scan can be expressed as a specific polynomial composed of the global uncertainty of the previous scan and the uncertainty introduced by the current scan matching. Due to space limitations, interested readers can refer to the method of applying the Baker-Campbell-Hausdorff (BCH) Formula (Mielnik et al. 1970) in (Barfoot et al. 2014).

#### 3. Experiment results

This section provides a detailed information of the experimental dataset and the evaluation of the effectiveness of proposed method.

# 3.1 Data description

We selected four routes from the NCLT dataset (Carlevaris-Bianco et al. 2016). Table 1 show some detailed description about these routes. The LiDAR used is Velodyne HDL-32E LIDAR. Each route is equipped with camera and IMU sensors. The ground truth is coming from RTK positioning results.

The ground truth is coming from KTK positioning results.						
Datas	Desciption					
et	Scenario	Trajectory	Time	Scan	LiDA	
		Length/m	Duratio	num	R type	
		_	n/s			
Seq1	Campus	1146.28	1025.3	10253	HDL-	
-	Road				32E	
Seq2	Campus	3201.98	2580.5	25805	HDL-	
	Road				32E	
Seq3	Campus	4107.57	3295.0	32950	HDL-	
•	Road				32E	
Seq4	Campus	4998.16	4110.5	41105	HDL-	
-	Road				32E	

Table 1 Detailed information about NCLT dataset

Four routes are all collected in the University of Michigan North Campus. Except for the Seq1 which was collected in cloudy weather, all other routes were collected in sunny weather.

# 3.2 Experiment Setup

In order to verify the effectiveness of our method, we set up fully comparative experiments. It is a common practice in current research to put the pose uncertainty obtained from scanto-scan matching as a constant. Usually, they use Monte Carlo to simulate the movement of a large number of initial particles under an assumption of pose uncertainty, and then evolve all possible distributions of particles in terms of global position. Moreover, to the best of our knowledge, there are few works on global positioning uncertainty estimation using real-world datasets. In this paper, we compare our proposed method with a benchmark method with constant uncertainty assumption of scan-to-scan matching and finally compare their real-time performances of global positioning uncertainty estimation.

**Evaluation criteria.** To evaluate the performance of the global positioning uncertainty estimation, we calculate the trajectory ATE (Sturm et al. 2012) of our SLAM framework. The closer the estimated positioning uncertainty is to the ATE, the better the performance. The calculation tool is EVO (Grupp. et al. 2017). The horizontal and vertical positioning uncertainty are calculated separately. The global uncertainty is:

$$\sigma_{hori} = \sqrt{U_{tx}^2 + U_{ty}^2}$$

$$\sigma_{vert} = \sqrt{U_{tz}^2}$$
(27)

Where  $U_{tx}^2$ ,  $U_{ty}^2$ ,  $U_{tz}^2$  are the corresponding diagonal elements of in the global uncertainty covariance matrix (18) after propagation in current scan.

**Implementation details:** All the experiments are implemented by C++ and tested on Ubuntu 20.04 LTS. The CPU is AMD Ryzen 7 5800H and 16G RAM.

Considering the simulation experiment parameters set in (Barfoot et al. 2014, Brossard et al. 2017), the benchmark method has a constant scan-to scan matching uncertainty matrix as:

$$\Sigma_{const} = diag \left( \begin{bmatrix} 10^{-6} & 10^{-6} & 10^{-6} & 10^{-4} & 10^{-4} & 10^{-4} \end{bmatrix} \right)$$
 (28)

# 3.3 Comparative Results

Figure 2 shows the route estimation results of four sequences. The APE shown in the figure is the result displayed by the EVO tool, and its meaning is consistent with ATE. Table 2 shows the ATE and maximum error of the four sequences.

Dataset	Not aligned mean ATE/max error (m)
Seq1	6.36/18.91
Seq2	12.93/23.25
Seq3	27.62/55.53
Seq4	16.53/42.56

Table 2 Comparison of the accuracy of not aligned trajectories

Figure 3 shows the global positioning uncertainty comparison of proposed method and the benchmark method for sequences 1-4, and the real trajectory ATE. In the left figure, the left 1-sigma circles represent the calculated global uncertainty, while the purple ones represent the global uncertainty calculated by constant scan matching uncertainty. From the figure, we can see that since the constant scan-to-scan matching uncertainty in the benchmark method is difficult to reflect the actual scan matching uncertainty, the global positioning uncertainty after multi scans propagation is very small and it is difficult to reflect the real tendency of ATE. Our method introduces MHSS to calculate more accurate scan-to-scan matching uncertainty. Therefore, the final global positioning uncertainty can envelop the real ATE, and is fully adaptive without the need to manually set prior parameters. At

the same time, the change trend of global uncertainty can also reflect the change trend of the real ATE. This can enable the graceful weighting of LiDAR SLAM with other positioning systems in multi-sensor fusion localization.

# 4. Conclusions

In this paper, we propose a self-adapting scan-to-scan matching uncertainty estimation method using MHSS, which enables the global uncertainty to propagate global positioning uncertainty over the SE(3) group. The MHSS method can

establish fault hypothesis and calculate state variance and variance difference. Compared with the benchmark method with constant scan-to-scan matching uncertainty using the NCLT dataset, our method can envelop the real SLAM ATE and can reflect the real changing tendency of ATE as well.

Future research will focus on integrating sensors such as IMU or GNSS into the SLAM framework, performing uncertainty analysis for each sensor to weight their positioning contributions.

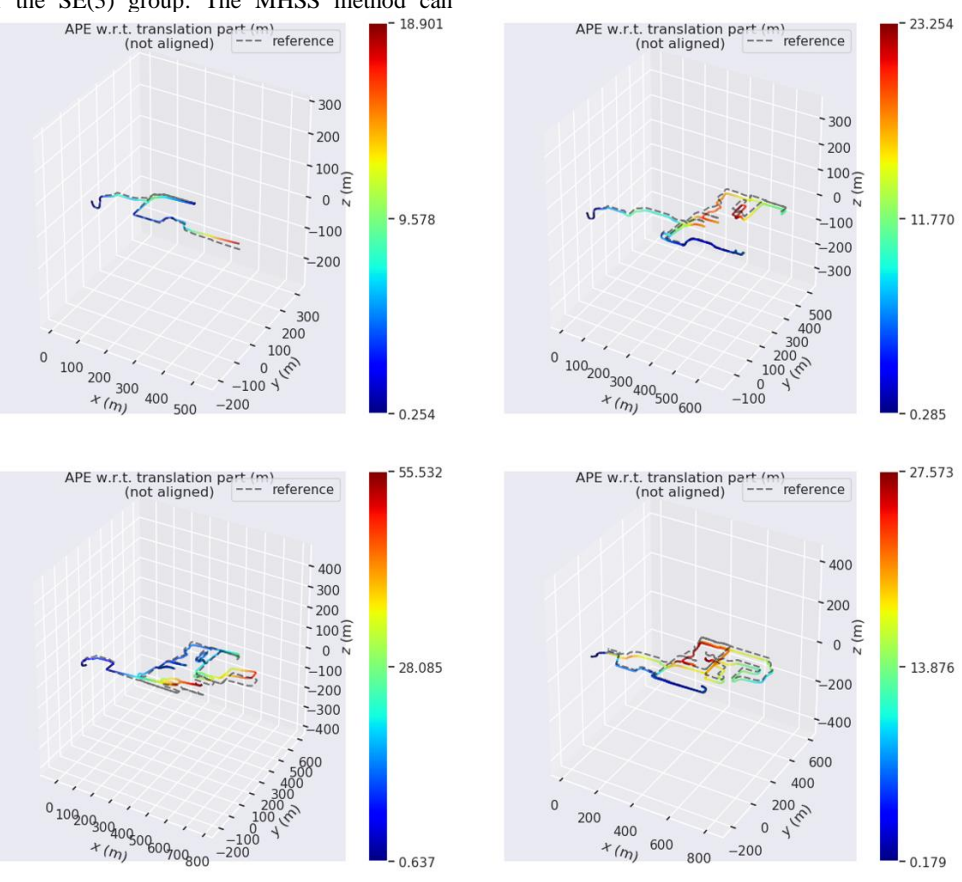
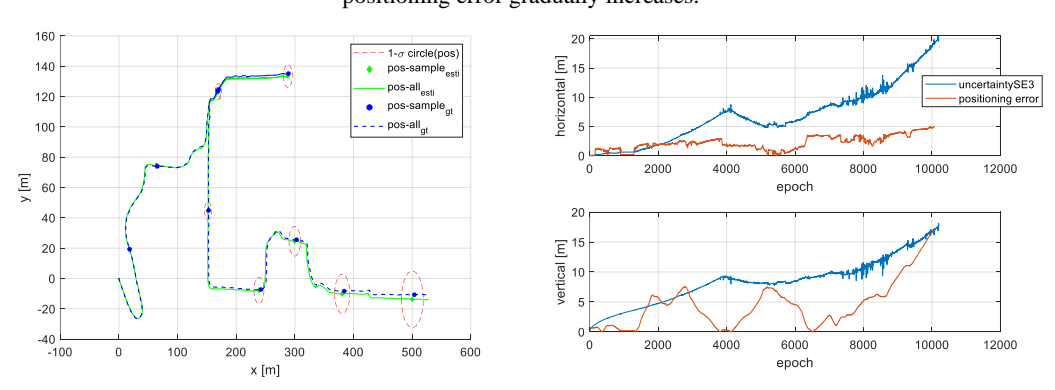


Figure 2. The real trajectory ATE of FAST-LIO for the four routes. The colorbar changes from blue to red, indicating that the positioning error gradually increases.



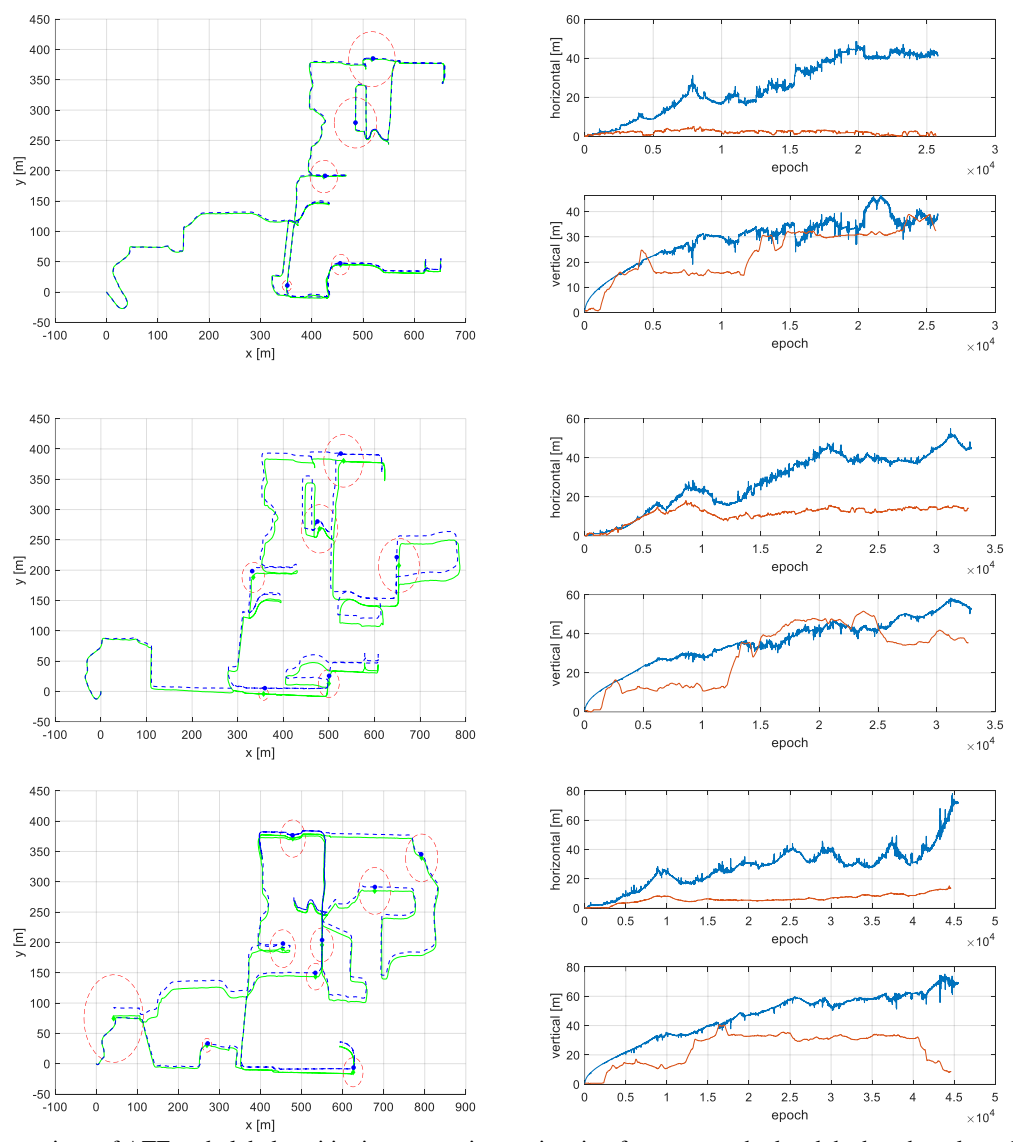


Figure 3. Comparison of ATE and global positioning uncertainty estimation from our method and the benchmark method. a, b, c, d represent the dataset sequence 1-4 respectively.

# References

Smith, R.C., Cheeseman, P., 1986. On the representation and estimation of spatial uncertainty. The international journal of Robotics Research 5, 56–68.

Macario Barros, A., Michel, M., Moline, Y., Corre, G., Carrel, F., 2022. A comprehensive survey of visual slam algorithms. Robotics 11, 24.

Zou, Q., Sun, Q., Chen, L., Nie, B., Li, Q., 2022. A Comparative Analysis of LiDAR SLAM-Based Indoor Navigation for Autonomous Vehicles. IEEE Transactions on Intelligent Transportation Systems 23, 6907–6921. https://doi.org/10.1109/TITS.2021.3063477

Tian, C., Liu, H., Liu, Z., Li, H., Wang, Y., 2023. Research on multi-sensor fusion SLAM algorithm based on improved gmapping. IEEE Access 11, 13690–13703.

Guo, S., Rong, Z., Wang, S., Wu, Y., 2022. A LiDAR SLAM with PCA-based feature extraction and two-stage matching.

IEEE Transactions on Instrumentation and Measurement 71, 1–11.

Tsai, T.-C., Peng, C.-C., 2024. Ground segmentation based point cloud feature extraction for 3D LiDAR SLAM enhancement. Measurement 236, 114890.

Cho, H., Kim, E.K., Kim, S., 2018. Indoor SLAM application using geometric and ICP matching methods based on line features. Robotics and Autonomous Systems 100, 206–224.

Chen, X., Läbe, T., Milioto, A., Röhling, T., Vysotska, O., Haag, A., Behley, J., Stachniss, C., 2021. OverlapNet: Loop

closing for LiDAR-based SLAM. arXiv preprint arXiv:2105.11344.

Chen, Y., Huang, S., Fitch, R., 2020. Active SLAM for mobile robots with area coverage and obstacle avoidance. IEEE/ASME Transactions on Mechatronics 25, 1182–1192.

- Zhang, J., Singh, S., others, 2014. LOAM: Lidar odometry and mapping in real-time., in: Robotics: Science and Systems. Berkeley, CA, pp. 1–9.
- Shan, T., Englot, B., 2018. Lego-loam: Lightweight and ground-optimized lidar odometry and mapping on variable terrain, in: 2018 IEEE/RSJ International Conference on Intelligent Robots and Systems (IROS). IEEE, pp. 4758–4765.
- Shan, T., Englot, B., Meyers, D., Wang, W., Ratti, C., Rus, D., 2020. Lio-sam: Tightly-coupled lidar inertial odometry via smoothing and mapping, in: 2020 IEEE/RSJ International Conference on Intelligent Robots and Systems (IROS). IEEE, pp. 5135–5142.
- Xu, W., Zhang, F., 2021. Fast-lio: A fast, robust lidar-inertial odometry package by tightly-coupled iterated kalman filter. IEEE Robotics and Automation Letters 6, 3317–3324.
- Xu, W., Cai, Y., He, D., Lin, J., Zhang, F., 2022. Fast-lio2: Fast direct lidar-inertial odometry. IEEE Transactions on Robotics 38, 2053–2073.
- Zheng, C., Zhu, Q., Xu, W., Liu, X., Guo, Q., Zhang, F., 2022. Fast-livo: Fast and tightly-coupled sparse-direct lidar-inertial-visual odometry, in: 2022 IEEE/RSJ International Conference on Intelligent Robots and Systems (IROS). IEEE, pp. 4003–4009.
- Zheng, C., Xu, W., Zou, Z., Hua, T., Yuan, C., He, D., Zhou, B., Liu, Z., Lin, J., Zhu, F., others, 2024. Fast-livo2: Fast, direct lidar-inertial-visual odometry. IEEE Transactions on Robotics.
- Talbot, W., Nash, J., Paton, M., Ambrose, E., Metz, B., Thakker, R., Etheredge, R., Ono, M., Ila, V., 2023. Principled ICP covariance modelling in perceptually degraded environments for the EELS mission concept, in: 2023 IEEE/RSJ International Conference on Intelligent Robots and Systems (IROS). IEEE, pp. 10763–10770.
- Smith, R., Self, M., Cheeseman, P., 1990. Estimating uncertain spatial relationships in robotics, in: Autonomous Robot Vehicles. Springer, pp. 167–193.
- Chirikjian, G.S., 2009. Stochastic Models, Information Theory, and Lie Groups, Volume 1: Classical Results and Geometric Methods. Springer Science & Business Media.
- Chirikjian, G.S., 2011. Stochastic models, information theory, and Lie groups, volume 2: Analytic methods and modern applications. Springer Science & Business Media.
- Barfoot, T.D., Furgale, P.T., 2014. Associating uncertainty with three-dimensional poses for use in estimation problems. IEEE Transactions on Robotics 30, 679–693.
- Brossard, M., Barrau, A., Chauchat, P., Bonnabel, S., 2021. Associating uncertainty to extended poses for on lie group imu preintegration with rotating earth. IEEE Transactions on Robotics 38, 998–1015.
- Mangelson, J.G., Ghaffari, M., Vasudevan, R., Eustice, R.M., 2020. Characterizing the uncertainty of jointly distributed poses in the lie algebra. IEEE Transactions on Robotics 36, 1371–1388.
- Blanch, J., Walter, T., Enge, P., Lee, Y., Pervan, B., Rippl, M., Spletter, A., 2012. Advanced RAIM user algorithm description:

- Integrity support message processing, fault detection, exclusion, and protection level calculation, in: Proceedings of the 25th International Technical Meeting of The Satellite Division of the Institute of Navigation (ION GNSS 2012). pp. 2828–2849.
- Blanch, J., Walker, T., Enge, P., Lee, Y., Pervan, B., Rippl, M., Spletter, A., Kropp, V., 2015. Baseline advanced RAIM user algorithm and possible improvements. IEEE Transactions on Aerospace and Electronic Systems 51, 713–732.
- Mielnik, B., Plebański, J., 1970. Combinatorial approach to baker-campbell-hausdorff exponents, in: Annales de l'institut Henri Poincaré. Section A, Physique Théorique. pp. 215–254.
- Sturm, J., Engelhard, N., Endres, F., Burgard, W., Cremers, D., 2012. A benchmark for the evaluation of RGB-D SLAM systems, in: 2012 IEEE/RSJ International Conference on Intelligent Robots and Systems. IEEE, pp. 573–580.
- Grupp, M., 2017. evo: Python package for the evaluation of odometry and SLAM.
- Carlevaris-Bianco, N., Ushani, A.K., Eustice, R.M., 2016. University of Michigan North Campus long-term vision and lidar dataset. The International Journal of Robotics Research 35, 1023–1035.